



1 **Winter observations of ClNO<sub>2</sub> in northern China: Spatiotemporal variability and**  
2 **insights into daytime peaks**

3 Men Xia<sup>1</sup>, Xiang Peng<sup>1</sup>, Weihao Wang<sup>1,8</sup>, Chuan Yu<sup>1,2</sup>, Zhe Wang<sup>6</sup>, Yee Jun Tham<sup>7</sup>,  
4 Jianmin Chen<sup>4</sup>, Hui Chen<sup>4</sup>, Yujing Mu<sup>5</sup>, Chenglong Zhang<sup>5</sup>, Pengfei Liu<sup>5</sup>, Likun Xue<sup>2</sup>,  
5 Xinfeng Wang<sup>2</sup>, Jian Gao<sup>3</sup>, Hong Li<sup>3</sup>, and Tao Wang<sup>1</sup>

6 <sup>1</sup>Department of Civil and Environmental Engineering, The Hong Kong Polytechnic  
7 University, Hong Kong SAR, China

8 <sup>2</sup>Environment Research Institute, Shandong University, Ji'nan, Shandong, China

9 <sup>3</sup>Chinese Research Academy of Environmental Sciences, Beijing, China

10 <sup>4</sup>Department of Environmental Science and Engineering, Fudan University, Institute of  
11 Atmospheric Sciences, Shanghai, China

12 <sup>5</sup>Research Center for Eco-Environmental Sciences, Chinese Academy of Sciences,  
13 Beijing, China

14 <sup>6</sup>Division of Environment and Sustainability, Hong Kong University of Science and  
15 Technology, Hong Kong SAR, China

16 <sup>7</sup>Institute for Atmospheric and Earth System Research/Physics, University of Helsinki,  
17 Helsinki, Finland

18 <sup>8</sup>Hangzhou PuYu Technology Development Co., Ltd, Hangzhou, Zhejiang, China

19 Correspondence: Tao Wang (cetwang@polyu.edu.hk)

20

21 **Abstract**

22 Nitryl chloride (ClNO<sub>2</sub>) is an important chlorine reservoir in the atmosphere that affects  
23 the oxidation of volatile organic compounds (VOCs) and the production of RO<sub>x</sub> radicals  
24 and ozone (O<sub>3</sub>). This study presents measurements of ClNO<sub>2</sub> and related compounds at  
25 urban, rural, and mountain sites in the winter of 2017–2018 over the North China Plain  
26 (NCP). The nocturnal concentrations of ClNO<sub>2</sub> were lower at the urban and rural sites  
27 but higher at the mountain site. The winter concentrations of ClNO<sub>2</sub> were generally  
28 lower than the summer concentrations that were previously observed at these sites,  
29 which was due to the lower nitrate radical (NO<sub>3</sub>) production rate ( $P(\text{NO}_3)$ ) and the  
30 smaller N<sub>2</sub>O<sub>5</sub> uptake coefficients ( $\gamma(\text{N}_2\text{O}_5)$ ) in winter, despite the higher dinitrogen  
31 pentoxide (N<sub>2</sub>O<sub>5</sub>) to NO<sub>3</sub> ratios in winter. Significant daytime peaks of ClNO<sub>2</sub> were  
32 observed at all the sites during the winter campaigns, with ClNO<sub>2</sub> mixing ratios of up  
33 to 1.3 ppbv. Vertical transport of ClNO<sub>2</sub> from the residual layers and prolonged  
34 photochemical lifetime of ClNO<sub>2</sub> in winter may explain the elevated daytime  
35 concentrations. The daytime-averaged chlorine radical (Cl) production rates ( $P(\text{Cl})$ )  
36 from the daytime ClNO<sub>2</sub> were 0.17, 0.11, and 0.12 ppbv h<sup>-1</sup> at the rural, urban, and  
37 mountain sites, respectively, which were approximately 3–4 times higher than the  
38 campaign-averaged conditions. Box model calculations showed that the Cl atoms  
39 liberated during the daytime peaks of ClNO<sub>2</sub> increased the RO<sub>x</sub> levels by up to 27–37 %  
40 and increased the daily O<sub>3</sub> productions by up to 13–18 %.

41

42 **Key points:**

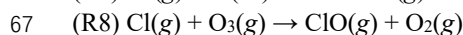
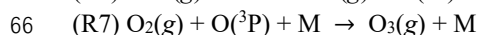
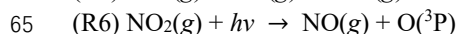
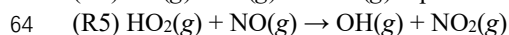
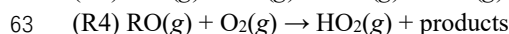
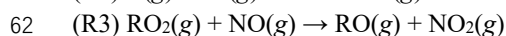
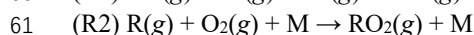
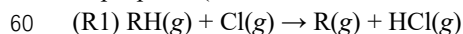
43 1. Winter measurements of ClNO<sub>2</sub> concentrations were made at rural, urban, and



- 44 mountain sites in northern China.  
45 2. The elevated daytime mixing ratios of ClNO<sub>2</sub> were up to 1.3 ppbv.  
46 3. The daytime peaks of ClNO<sub>2</sub> increased the concentration of RO<sub>x</sub> radicals by up to  
47 27–37 % and the net O<sub>3</sub> production by 13–18 %.

## 49 1. Introduction

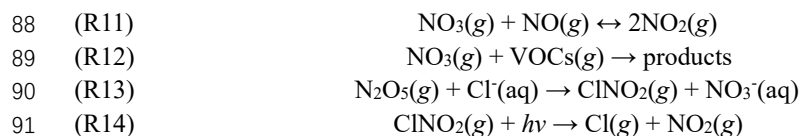
50 Cl is a potent atmospheric oxidant that reacts analogously to hydroxyl radicals (OH)  
51 with hydrocarbons (Wang et al., 2019b). Cl is highly reactive toward alkanes, with the  
52 rate constants of its reactions with alkanes being approximately 10–200 times greater  
53 than some of the OH + VOCs reactions (Atkinson and Arey, 2003; Burkholder et al.,  
54 2015). Consequently, Cl enhances the production of RO<sub>x</sub> (= OH + HO<sub>2</sub> + RO<sub>2</sub>) via  
55 Reactions R1–R4, which promotes O<sub>3</sub> formation by converting nitric oxide (NO) to  
56 nitrogen dioxide (NO<sub>2</sub>) (Reactions R3 and R5). Cl also consumes O<sub>3</sub> via Reaction R8.  
57 The net effect of the reactivity of Cl is typically the depletion of O<sub>3</sub> in the stratosphere  
58 (Molina and Rowland, 1974) and an increase in O<sub>3</sub> production in the polluted  
59 troposphere (Riedel et al., 2014; Xue et al., 2015).



68 where M denotes the third body in ambient air.

69  
70 The production of Cl is determined by the formation and decomposition of Cl  
71 precursors such as ClNO<sub>2</sub> (Chang et al., 2011). ClNO<sub>2</sub> is produced mostly in dark  
72 conditions by the heterogeneous uptake of N<sub>2</sub>O<sub>5</sub> on chloride (Cl<sup>-</sup>)-laden aerosols  
73 (Reactions R9–R13) and undergoes photolysis during the day (Reaction R14)  
74 (Finlayson-Pitts et al., 1989). ClNO<sub>2</sub> formation is constrained by the NO<sub>3</sub> production  
75 rate ( $P(\text{NO}_3)$ , Reaction R9). NO<sub>3</sub> is in thermal equilibrium with N<sub>2</sub>O<sub>5</sub> (Reaction R10),  
76 and the equilibrium constant ( $K_{\text{eq}}$ ) depends on temperature and NO<sub>2</sub> concentrations.  
77 N<sub>2</sub>O<sub>5</sub> formation is suppressed by NO and VOCs as they consume NO<sub>3</sub> (Reactions R11–  
78 12). The N<sub>2</sub>O<sub>5</sub> uptake probability ( $\gamma(\text{N}_2\text{O}_5)$ ) and ClNO<sub>2</sub> production yield ( $\varphi(\text{ClNO}_2)$ )  
79 are kinetic parameters with values between 0 and 1, which can be derived from the  
80 observation data of N<sub>2</sub>O<sub>5</sub>, ClNO<sub>2</sub>, and related species (Brown et al., 2006; Phillips et  
81 al., 2016). Previous laboratory studies have demonstrated that  $\gamma(\text{N}_2\text{O}_5)$  is enhanced by  
82 higher relative humidity (RH) and particulate Cl<sup>-</sup> concentrations but suppressed by  
83 higher temperature and concentrations of aerosol nitrate (NO<sub>3</sub><sup>-</sup>) and organic species  
84 (Behnke et al., 1997; Hallquist et al., 2003; Bertram et al., 2009; Griffiths and Anthony  
85 Cox, 2009).





92  
93 Field observations of ClNO<sub>2</sub> were first reported in the marine boundary layer off the  
94 coast of the Houston-Galveston area in the USA (Osthoff et al., 2008). Subsequent  
95 studies demonstrated the worldwide ubiquity of ClNO<sub>2</sub> and confirmed its significant  
96 role in photochemistry (Thornton et al., 2010; Mielke et al., 2011; Phillips et al., 2012;  
97 Edwards et al., 2013; Bannan et al., 2015; Wild et al., 2016; Wang et al., 2016;  
98 Bannan et al., 2019; Eger et al., 2019). The role of ClNO<sub>2</sub> in the radical budget could  
99 be more important than that of OH in winter, because OH production is reduced in  
100 winter owing to lower concentrations of O<sub>3</sub> and H<sub>2</sub>O vapor in this season (Haskins et  
101 al., 2019). A limited number of winter observations of ClNO<sub>2</sub> have been conducted on  
102 various platforms, including on aircrafts over northern Europe (Priestley et al., 2018)  
103 and the eastern US (Haskins et al., 2019), on a tall tower in Boulder, USA (Riedel et al.,  
104 2013), on a mountain top in Hong Kong (Wang et al., 2016), and at ground sites in  
105 Alberta, Canada (Mielke et al., 2016) and Heshan, China (Yun et al., 2018). These  
106 studies found high ClNO<sub>2</sub> mixing ratios of up to 7.7 ppbv (Yun et al., 2018) in winter  
107 and a contribution of ClNO<sub>2</sub> to Cl liberation of up to 83 % (Priestley et al., 2018).

108  
109 The chemical production of ClNO<sub>2</sub> in winter has some unique features compared  
110 with that in warmer seasons. Long winter nights provide more time for ClNO<sub>2</sub>  
111 production and accumulation. Lower temperatures in winter shift the N<sub>2</sub>O<sub>5</sub>-NO<sub>3</sub>  
112 equilibrium to the N<sub>2</sub>O<sub>5</sub> side (Brown et al., 2003) and increase the  $\gamma(\text{N}_2\text{O}_5)$  on aerosols  
113 (Bertram and Thornton, 2009). However,  $P(\text{NO}_3)$  might be lower in winter due to  
114 reduced O<sub>3</sub> concentrations. The availability of aerosol Cl<sup>-</sup> also varies in winter and  
115 summer. The winter monsoon brings air masses from the interior of the continent,  
116 thereby suppressing the transport of sea salt to inland areas. However, more Cl<sup>-</sup> is  
117 emitted due to coal burning in winter (McCulloch et al., 1999; Fu et al., 2018). Thus,  
118 considering the complexity of N<sub>2</sub>O<sub>5</sub> chemistry and Cl<sup>-</sup> sources, it is not clear whether  
119 ClNO<sub>2</sub> formation is more prevalent in winter.

120  
121 The North China Plain (NCP) – home to Beijing and several other megacities – is  
122 one of the most industrialized and populous regions of China, and frequently suffers  
123 from severe haze pollution in winter (An et al., 2019; Fu et al., 2020). ClNO<sub>2</sub>  
124 concentrations have been measured over the NCP (Breton et al., 2018; Zhou et al.,  
125 2018), but only one study was conducted in winter (Breton et al., 2018). This study  
126 presents recent field observations of ClNO<sub>2</sub> concentrations from three campaigns  
127 conducted in winter and early spring at three sites in the NCP. The results were  
128 compared with those obtained in the previous summer campaigns at the same locations.  
129 We examined the factors controlling ClNO<sub>2</sub> formation, i.e.,  $P(\text{NO}_3)$ , the nocturnal  
130 reactivity of NO<sub>3</sub> and N<sub>2</sub>O<sub>5</sub>,  $\gamma(\text{N}_2\text{O}_5)$ , and  $\phi(\text{ClNO}_2)$ . We then focused on the  
131 unexpected daytime peaks of ClNO<sub>2</sub> concentrations that were observed at the sites and



132 evaluated their impact on the daytime atmospheric oxidative capacity using a chemical  
133 box model.

134

## 135 2. Methods

### 136 2.1 Observation sites

137 Field campaigns were performed in Wangdu, Beijing, and Mt. Tai in sequence during  
138 the winter-early spring of 2017–2018 (Table 1). The locations of the three sites are  
139 shown in Fig. S1. The sites were selected for investigation of ClNO<sub>2</sub> in urban, rural,  
140 and mountain areas of the NCP. The winter indoor-heating period lasts from early  
141 November to 15 March of the following year (Ran et al., 2016), and thus the  
142 observations were made mostly during the heating period during which coal is  
143 intensively used. Detailed descriptions of the measurement sites are available in  
144 previous studies (Tham et al., 2016; Wang et al., 2017c; Xia et al., 2019), and a brief  
145 introduction is given here.

146

147 Table 1. Locations and periods of the field campaigns relevant to this study.

Location	Site category	Season	Observation period	Coordinate
Wangdu	Rural	Winter <sup>1</sup>	9-31 December 2017	38.66° N, 115.25° E
		Summer <sup>2</sup>	21 June to 9 July 2014	38.67° N, 115.20° E
Beijing	Urban	Winter <sup>1</sup>	6 January to 1 February 2018	40.04° N, 116.42° E
		Early summer <sup>3</sup>	24 April to 31 May 2017	116.42° E
Mt. Tai	Mountain	Winter to early spring <sup>1</sup>	7 March to 8 April 2018	36.25°N, 117.10°E
		Summer <sup>4</sup>	24 July to 27 August 2014	

148 <sup>1</sup>Observations from this study.

149 <sup>2-4</sup>Observations from previous studies, i.e., Tham et al. (2016), Xia et al. (2019), and  
150 Wang et al. (2017c), respectively.

151

152 Our observations at the Wangdu site were part of the Campaign of Oxidation  
153 Potential Research for air Pollution in winter (COPPER). The Wangdu site is located in  
154 Dongbaituo Village, Hebei Province. Local villagers use coal stoves for cooking and  
155 heating during winter. National road G4 and provincial road S335 are 1 km and 3 km  
156 to the west of the sampling site, respectively. Many heavy-duty trucks passed through  
157 G4 and S335 every night during the study period, emitting a large amount of NO<sub>x</sub> and  
158 particulate matters. Therefore, the site experienced heavy pollution from coal burning  
159 and road traffic (Peng et al., 2020).

160

161 The Beijing site is located at the Chinese Research Academy of Environmental  
162 Science (CRAES), which is 15 km northeast of the city center. The sampling site is  
163 surrounded by intra-city roads, commercial buildings, and residential buildings with



164 few industrial facilities. When the prevailing wind originates from the north (i.e.,  
165 remote mountainous regions), the site is upwind from the Beijing downtown area and  
166 thus is less polluted. However, when the wind originates from the south, the site  
167 receives pollutants from Beijing's urban areas in the NCP (Xia et al., 2019).

168  
169 Mt. Tai is located approximately 40 km south of Jinan City (population: 8.9 million)  
170 and 15 km north of Tai'an City (population: 5.6 million) (Wen et al., 2018).  
171 Measurements were taken at Mt. Tai meteorological station (1534 m a.s.l.). The site is  
172 isolated from the anthropogenic emissions of tourist areas and is not affected by local  
173 emissions. The observation period, i.e., March to April, was in early spring in the NCP.  
174 However, considering the low temperature ( $4.6 \pm 6.3$  °C) observed on top of Mt. Tai,  
175 this study considered the observation period as winter to early spring.

## 176 2.2 Measurements of N<sub>2</sub>O<sub>5</sub> and ClNO<sub>2</sub> concentrations

177 N<sub>2</sub>O<sub>5</sub> and ClNO<sub>2</sub> were simultaneously measured by a chemical ionization mass  
178 spectrometer with a quadrupole mass analyzer (Q-CIMS; THS Instruments). The  
179 principles and calibrations of the Q-CIMS measurements are available in previous  
180 studies (Tham et al., 2016; Wang et al., 2017c; Xia et al., 2019). The primary ions used  
181 in the Q-CIMS were iodide (I<sup>-</sup>) and its water clusters, which were generated using CH<sub>3</sub>I  
182 with an inline ionizer (<sup>210</sup>Po). The iodide adducts, namely IN<sub>2</sub>O<sub>5</sub><sup>-</sup> and IClNO<sub>2</sub><sup>-</sup>, were  
183 then detected by the mass spectrometer. An example of the mass spectrum is shown in  
184 Fig. S2. The isotopic ratios of I<sup>35</sup>ClNO<sub>2</sub><sup>-</sup> and I<sup>37</sup>ClNO<sub>2</sub><sup>-</sup> in the ambient data were used  
185 to confirm the identity of ClNO<sub>2</sub> (Fig. S3). Gas-phase mixtures of NO<sub>2</sub> and O<sub>3</sub> produced  
186 N<sub>2</sub>O<sub>5</sub> in a dynamic gas calibrator (Sabio Instruments) for N<sub>2</sub>O<sub>5</sub> calibration. The  
187 synthetic N<sub>2</sub>O<sub>5</sub> was converted to ClNO<sub>2</sub> by passage through a humidified NaCl slurry  
188 for ClNO<sub>2</sub> calibration. On-site calibrations were performed every 1–2 days, and  
189 background detections of N<sub>2</sub>O<sub>5</sub> and ClNO<sub>2</sub> were conducted every day by passing  
190 ambient air through glass wool. The dependence of the N<sub>2</sub>O<sub>5</sub> sensitivities (normalized  
191 to the signal of I(H<sub>2</sub>O)<sup>-</sup>) on ambient RH was tested and used to calibrate the N<sub>2</sub>O<sub>5</sub> data  
192 (Fig. S4). The normalized sensitivity of N<sub>2</sub>O<sub>5</sub> is the signal ratio of I(N<sub>2</sub>O<sub>5</sub>)<sup>-</sup>  
193 in the presence of 1 pptv of N<sub>2</sub>O<sub>5</sub>. The normalized sensitivities and detection limits of  
194 the N<sub>2</sub>O<sub>5</sub> and ClNO<sub>2</sub> measurements were  $(0.9\text{--}2.2) \times 10^{-5}$  Hz/Hz/pptv and 4–7 pptv ( $3\sigma$   
195 in 5 minutes), respectively during the three campaigns. The variation in the sensitivities  
196 and detection limits of N<sub>2</sub>O<sub>5</sub> and ClNO<sub>2</sub> were small within each campaign (Text S1,  
197 Table S1, and Fig. S5). A virtual-impactor design (Peng et al., 2020) was adopted, and  
198 the sampling tube was replaced daily to minimize inlet artifacts.

199

## 200 2.3 Other measurements

201 The trace gases, particle number size distribution (PNSD), ionic composition of  
202 aerosols and other species were simultaneously measured (Table S2). Online VOCs  
203 measurements were performed by gas chromatography-flame-ionization  
204 detection/mass spectrometry (GC-FID/MS; Chromatotec Group) at the Beijing site  
205 (Zhang et al., 2017) and Wangdu site (Zhang et al., 2020). At Mt. Tai, we used canisters  
206 to collect air samples, which were analyzed using GC-FID/MS. The ionic compositions  
207



208 of PM<sub>2.5</sub> (e.g., NH<sub>4</sub><sup>+</sup>, NO<sub>3</sub><sup>-</sup>, SO<sub>4</sub><sup>2-</sup>, and Cl<sup>-</sup>) were quantified by the Monitor for AeRosols  
209 and GAses in ambient air (MARGA, Metrohm) at the Beijing and Mt. Tai sites (Wen  
210 et al., 2018). An aerosol chemical speciation monitor (ACSM, Aerodyne Research Inc.)  
211 was utilized at the Wangdu site to monitor the non-refractory components of these ions.  
212 The concentrations of the NO<sub>3</sub><sup>-</sup>, SO<sub>4</sub><sup>2-</sup>, and NH<sub>4</sub><sup>+</sup> measured simultaneously by the  
213 MARGA and ACSM were in good agreement, whereas the concentration of Cl<sup>-</sup>  
214 measured by the ACSM was slightly lower than that measured by the MARGA, which  
215 was possibly due to the significant proportion of refractory chloride, e.g., NaCl, present  
216 in the aerosols (Xia et al., 2020). We assumed that the particles sampled by a wide-  
217 range particle spectrometer (WPS) were spherical in shape and calculated the aerosol  
218 surface area density (S<sub>a</sub>) and volume density (V<sub>a</sub>). A parameterization was adopted to  
219 consider the hygroscopic growth factor (GF) of aerosol sizes, as follows:

220  $GF = a \times \left(b + \frac{1}{1-RH}\right)^{1/3}$  (Lewis, 2008), where the parameters a and b were derived as  
221 0.582 and 8.460, respectively in a previous field study over the NCP (Achtert et al.,  
222 2009).

223  
224 2.4 Calculation of N<sub>2</sub>O<sub>5</sub> loss and ClNO<sub>2</sub> production

225 Some analytical metrics were estimated from the observation data. *P*(NO<sub>3</sub>) was  
226 calculated using Eq. (1), where *k*<sub>1</sub> represents the rate constant of Reaction R9.

227 (Eq. 1)  $P(\text{NO}_3) = k_1 \times [\text{O}_3] \times [\text{NO}_2]$

228 *k*(NO<sub>3</sub>) during the night was estimated using the measured mixing ratios of NO and  
229 VOCs.

230 (Eq. 2)  $k(\text{NO}_3) = \sum k_i [\text{VOC}_i] + k_{\text{NO}+\text{NO}_3} [\text{NO}]$

231 where *k*<sub>*i*</sub> is the rate constant for a specific VOC + NO<sub>3</sub> reaction and *k*<sub>NO+NO<sub>3</sub></sub> represents  
232 the rate constant for Reaction R11. The ambient concentrations of NO<sub>3</sub> were estimated  
233 by assuming that NO<sub>3</sub> and N<sub>2</sub>O<sub>5</sub> were in dynamic equilibrium.

234 (Eq. 3)  $[\text{NO}_3] = \frac{[\text{N}_2\text{O}_5]}{[\text{NO}_2]K_{\text{eq}}}$

235 The loss rates of NO<sub>3</sub> due to NO and VOCs were then calculated by *k*<sub>NO+NO<sub>3</sub></sub>[NO][NO<sub>3</sub>]  
236 and  $\sum k_i [\text{VOC}_i][\text{NO}_3]$ , respectively.

237 The loss rate coefficient of N<sub>2</sub>O<sub>5</sub> on the aerosol surface (*k*(N<sub>2</sub>O<sub>5</sub>)) is expressed as  
238 follows.

239 (Eq. 4)  $k(\text{N}_2\text{O}_5) = 0.25 \times c(\text{N}_2\text{O}_5) \times S_a \times \gamma(\text{N}_2\text{O}_5)$

240 where *c*(N<sub>2</sub>O<sub>5</sub>) represents the average molecular velocity of N<sub>2</sub>O<sub>5</sub>. The rate constants  
241 (*k*<sub>1</sub>, *k*<sub>*i*</sub>, and *k*<sub>NO+NO<sub>3</sub></sub>) and equilibrium constant (*K*<sub>eq</sub>) are calculated as temperature-  
242 dependent parameters.

243  
244  $\gamma(\text{N}_2\text{O}_5)$  and  $\phi(\text{ClNO}_2)$  were estimated using steady-state analysis in applicable cases  
245 (Brown et al., 2006). This method assumes a steady state of N<sub>2</sub>O<sub>5</sub>, which means that



246 the production rate of  $\text{N}_2\text{O}_5$  is equal to its loss rate. We adopted the criteria described  
247 by Xia et al. (2020) to select the cases, namely low concentrations of  $\text{NO}$ , an increasing  
248 trend of  $\text{ClNO}_2$  concentrations, and stable air masses. Equation (5) was then established  
249 by plotting  $\tau(\text{N}_2\text{O}_5)^{-1} \times [\text{NO}_2] \times K_{\text{eq}}$  against  $0.25 \times S_a \times C_{\text{N}_2\text{O}_5} \times [\text{NO}_2] \times K_{\text{eq}}$ , with  
250  $\gamma(\text{N}_2\text{O}_5)$  as the slope and  $k(\text{NO}_3)$  as the intercept in the linear regression (Brown et al.,  
251 2003). Here, the derived  $\gamma(\text{N}_2\text{O}_5)$  was accepted when the regression had  $R^2 > 0.5$  and  
252  $k(\text{NO}_3) > 0$ .

253 (Eq. 5)  $\tau(\text{N}_2\text{O}_5)^{-1} \times K_{\text{eq}} \times [\text{NO}_2] \approx 0.25 \times C_{\text{N}_2\text{O}_5} \times S_a \times K_{\text{eq}} \times [\text{NO}_2] \times \gamma(\text{N}_2\text{O}_5) + k(\text{NO}_3)$   
254  $\phi(\text{ClNO}_2)$  was then calculated using the following equation:

255 (Eq. 6) 
$$\phi(\text{ClNO}_2) = \frac{d[\text{ClNO}_2]/dt}{k(\text{N}_2\text{O}_5)[\text{N}_2\text{O}_5]}$$

256 where  $d[\text{ClNO}_2]/dt$  and  $[\text{N}_2\text{O}_5]$  represent the increasing rate of  $\text{ClNO}_2$  production and  
257 the average concentration of  $\text{N}_2\text{O}_5$ , respectively within the selected cases.

258

## 259 2.5 Box model

260 An observation-based chemical box model was utilized to simulate the  
261 concentrations of  $\text{Cl}$  and  $\text{RO}_x$  radicals and the production and loss pathways of  $\text{O}_3$ . The  
262 detailed model description is available in Peng et al. (2020). Based on Master Chemical  
263 Mechanism (MCM) v3.3.1 (Jenkin et al., 2015), Peng et al. (2020) modified the  
264 chemical mechanisms to include up-to-date gas-phase chlorine and bromine chemistry.  
265 The observed  $\text{N}_2\text{O}_5$ ,  $\text{ClNO}_2$ ,  $\text{NO}_x$ ,  $\text{HONO}$ ,  $\text{O}_3$ ,  $j\text{NO}_2$ , and related species were  
266 constrained in the model for every 10 minutes of model time, after interpolating or  
267 averaging the data (Table S3). The mixing ratios of oxygenated volatile organic  
268 compounds (OVOCs) and VOCs (Section 2.3) were constrained every hour. We  
269 assumed the mixing ratio of  $\text{CH}_4$  to be constant at 2000 ppbv (Tan et al., 2017). The  
270 photolysis frequencies of  $\text{ClNO}_2$ ,  $\text{O}_3$ , and other species were simulated according to the  
271 solar zenith angle using the Tropospheric Ultraviolet and Visible (TUV) Radiation  
272 model and scaled by the observed  $j\text{NO}_2$  values. Numerical experiments were conducted  
273 by constraining (Case 1) and not constraining  $\text{ClNO}_2$  data (Case 2) at each site. The  
274 differences in the radical concentrations and  $\text{O}_3$  budgets between Cases 1 and 2  
275 represented the effect of  $\text{ClNO}_2$ . For example, the increase in  $\text{RO}_x$  (%) due to  $\text{ClNO}_2$   
276 was calculated by  $(\text{RO}_x_{\text{w}} - \text{RO}_x_{\text{wo}}) / \text{RO}_x_{\text{wo}}$ , where  $\text{RO}_x_{\text{w}}$  represents the  
277 concentration of  $\text{RO}_x$  in Case 1 with  $\text{ClNO}_2$  constrained in the model and  $\text{RO}_x_{\text{wo}}$   
278 represents the concentration of  $\text{RO}_x$  in Case 2 without  $\text{ClNO}_2$  constrained.

279

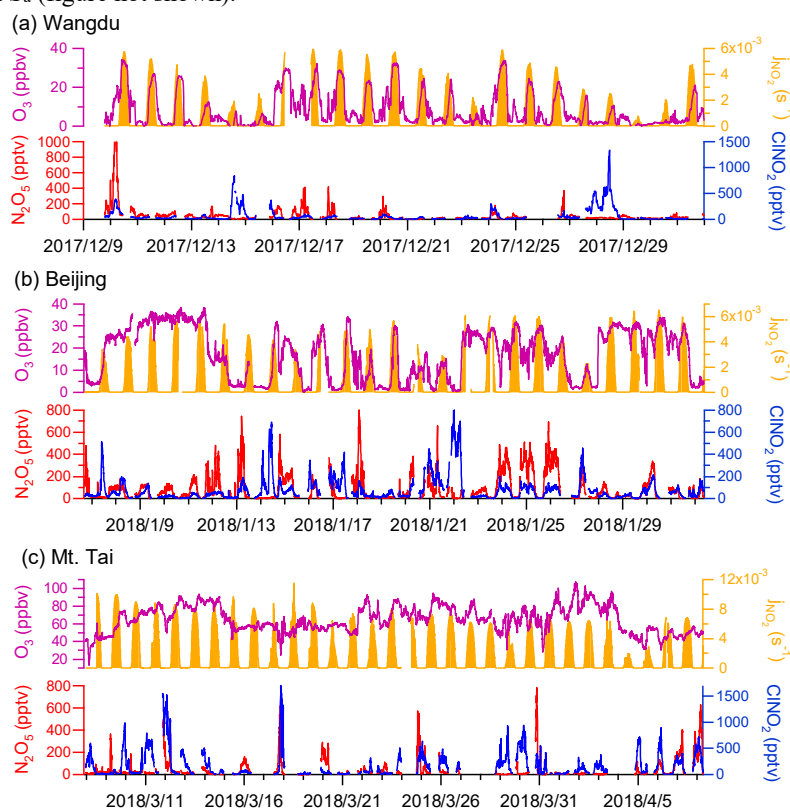
## 280 3. Results

### 281 3.1 Overall measurements, diurnal patterns and comparison with other studies

282 The time series of  $\text{N}_2\text{O}_5$  and  $\text{ClNO}_2$  levels in the three campaigns are displayed in  
283 Fig. 1. Overall, elevated levels of  $\text{N}_2\text{O}_5$  and  $\text{ClNO}_2$  were observed with different  
284 patterns at each site. The ground sites (Wangdu and Beijing) were characterized by high  
285  $\text{NO}_x$  levels ( $83.2 \pm 81.3$  ppbv and  $35.6 \pm 27.3$  ppbv, respectively) and low  $\text{O}_3$  levels  
286 ( $8.5 \pm 8.8$  ppbv and  $17.3 \pm 11.4$  ppbv, respectively), whereas the mountain site, Mt. Tai,  
287 was marked by relatively lower  $\text{NO}_x$  levels ( $2.4 \pm 2.0$  ppbv) and higher  $\text{O}_3$  levels ( $64.6$   
288  $\pm 14.7$  ppbv) (Fig. S6). The campaign-averaged mixing ratios of  $\text{ClNO}_2$  were similar at



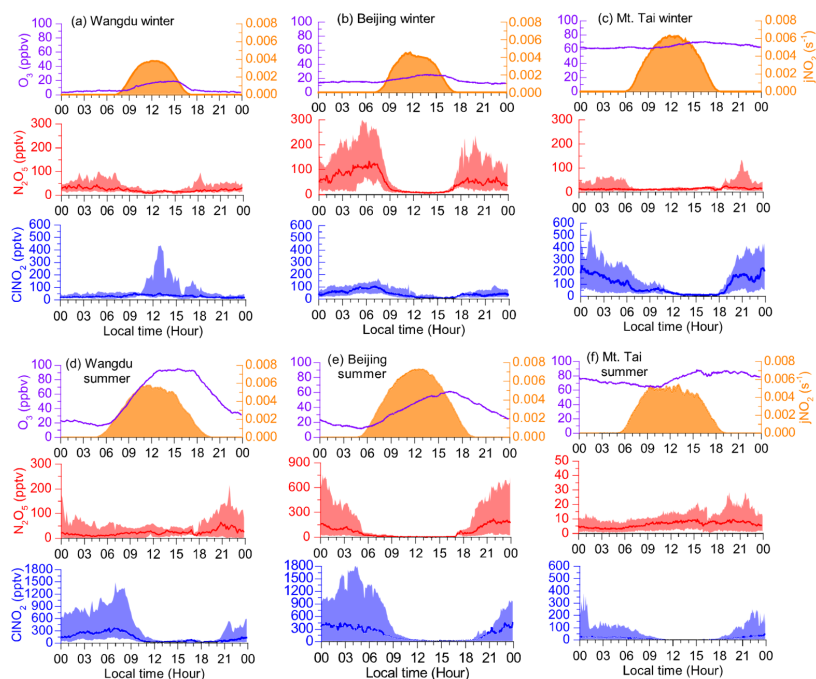
289 the ground sites ( $71 \pm 132$  pptv and  $76 \pm 103$  pptv in Wangdu and Beijing, respectively),  
290 and were significantly lower than that at Mt. Tai ( $179 \pm 247$  pptv). The nocturnal ratio  
291 of  $\text{ClNO}_2/\text{N}_2\text{O}_5$  at each site displayed large day-to-day variability, which was positively  
292 dependent on the ambient RH (Fig. S7) and, to a lesser extent, positively correlated  
293 with  $S_a$  (figure not shown).



294  
295 **Figure 1.** Overall observations of  $\text{N}_2\text{O}_5$ ,  $\text{ClNO}_2$  and related species at the (a) Wangdu,  
296 (b) Beijing, and (c) Mt. Tai sites.

297  
298 The campaign-averaged diurnal patterns of the mixing ratios of  $\text{N}_2\text{O}_5$ ,  $\text{ClNO}_2$ , and  
299 related species are depicted in Fig. 2.  $\text{ClNO}_2$  levels typically exhibited a daily cycle,  
300 peaking at night and decreasing during the day. The diurnal pattern of  $\text{ClNO}_2$  at the  
301 Wangdu site in winter was an exception, with elevated concentrations (10–90  
302 percentiles) around midday (12:00–14:00 local time; LT), which resulted from a  
303 noontime peak in  $\text{ClNO}_2$  concentrations during a few days at Wangdu. The detailed  
304 observation results from each site are separately introduced as follows.





305  
306 **Figure 2.** Diurnal average levels of N<sub>2</sub>O<sub>5</sub>, ClNO<sub>2</sub>, O<sub>3</sub>, and jNO<sub>2</sub> observed at the Wangdu,  
307 Beijing, and Mt. Tai sites throughout the campaign in winter (this study) and previous  
308 summer field studies (Table 1). The shaded areas indicate the 10th and 90th percentiles.  
309

310 The nocturnal production of ClNO<sub>2</sub> was insignificant in Wangdu despite the presence  
311 of abundant Cl<sup>-</sup> ( $3.3 \pm 3.2 \mu\text{g m}^{-3}$  throughout the observation), which likely originated  
312 from the intensive residential coal combustion in the area (Peng et al., 2020). The  
313 Wangdu site experienced high mass concentrations of PM<sub>2.5</sub> (a maximum of  
314 approximately  $450 \mu\text{g m}^{-3}$ ) and very large mixing ratios of NO (a maximum of  
315 approximately 350 ppbv). The wind rose analysis showed that the high concentrations  
316 of NO originated from the west of the sampling site where two major roads were located.  
317 Numerous heavy-duty trucks on these roads were responsible for high NO  
318 concentrations. The presence of abundant NO inhibited N<sub>2</sub>O<sub>5</sub> formation by consuming  
319 O<sub>3</sub> and NO<sub>3</sub> at the Wangdu site. When the ambient concentrations of NO substantially  
320 decreased, e.g., on 10 December, the N<sub>2</sub>O<sub>5</sub> mixing ratios increased to 1 ppbv. The  
321 mixing ratios of ClNO<sub>2</sub> were mostly low (< 200 pptv) during the night. However,  
322 significant daytime peaks in ClNO<sub>2</sub> mixing ratios were observed on 14 and 28  
323 December, reaching approximately 0.8 ppbv and 1.3 ppbv, respectively. The daytime  
324 peaks in ClNO<sub>2</sub> concentrations at the three sites are discussed in detail in Section 3.3.  
325 For comparison, the ambient mixing ratios of NO in the summer campaign at Wangdu  
326 were much lower (mostly 0-10 ppbv) and O<sub>3</sub> mixing ratios were much higher (i.e.,  
327 exceeded 90 ppbv on most days), which favored the production of N<sub>2</sub>O<sub>5</sub> and ClNO<sub>2</sub>  
328 (Tham et al., 2016).  
329



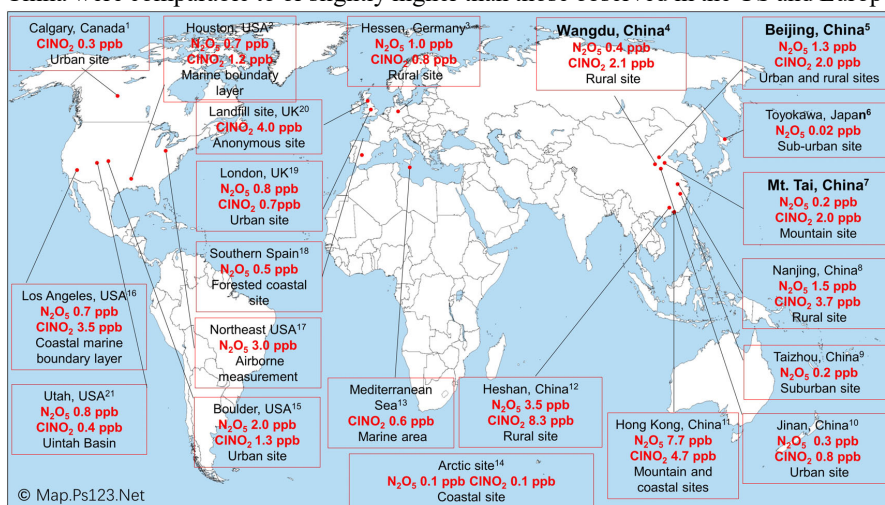
330 The winter Beijing observations showed that there was significant production of  
331  $\text{N}_2\text{O}_5$  but limited conversion of  $\text{N}_2\text{O}_5$  to  $\text{ClNO}_2$  in dry conditions. The observation  
332 period in Beijing was divided into polluted days ( $24\text{-h PM}_{2.5} > 75 \mu\text{g m}^{-3}$ ; China's Grade  
333 II air quality standard for  $\text{PM}_{2.5}$ ) and clean days ( $24\text{-h PM}_{2.5} < 35 \mu\text{g m}^{-3}$ ; Grade I  
334 standard). The polluted periods were characterized by simultaneous high levels of  $\text{PM}_{2.5}$   
335 and  $\text{NO}$ , e.g., on 19 January. The clean periods were marked by relatively high mixing  
336 ratios of  $\text{O}_3$ , low levels of  $\text{PM}_{2.5}$  and  $\text{NO}_x$ , e.g., from 8 to 11 January. Both polluted and  
337 clean conditions were unfavorable for  $\text{ClNO}_2$  formation owing to the high  
338 concentrations of  $\text{NO}$  on the polluted days and the low concentrations of  $\text{NO}_2$  and  
339 aerosols on the clean days. Moreover, the RH observed in Beijing was typically below  
340 40 %, which indicated relatively slow heterogeneous loss of  $\text{N}_2\text{O}_5$  and slow  $\text{ClNO}_2$   
341 formation. Consequently,  $\text{N}_2\text{O}_5$  mixing ratios frequently accumulated to elevated levels,  
342 exceeding 0.4 ppbv on 10 of the 26 observation nights, and the mixing ratio of  $\text{ClNO}_2$   
343 was mostly below 0.4 ppbv. The highest mixing ratios of  $\text{ClNO}_2$  were observed (up to  
344 approximately 0.8 ppbv) when the site occasionally intercepted air masses with a higher  
345 RH (approximately 75 %), e.g., on the night of 22 January. This result is similar to the  
346 previous observation in Beijing (Xia et al., 2019), in which the ratio of  $\text{ClNO}_2$  to  $\text{N}_2\text{O}_5$   
347 increased significantly from late spring with a low RH (10–30 %) to early summer with  
348 a higher RH (20–80 %). The overall mixing ratios of  $\text{ClNO}_2$  in the present Beijing study  
349 in winter were also significantly lower than those reported in summer (maximum of 1.4  
350 ppbv to 2.9 ppbv) in other studies (Breton et al., 2018; Zhou et al., 2018).

351  
352 Elevated mixing ratios of  $\text{ClNO}_2$  (i.e., above 0.5 ppbv) were frequently recorded at  
353 the Mt. Tai station. High concentrations of  $\text{PM}_{2.5}$  ( $34.5 \pm 27.3 \mu\text{g m}^{-3}$ ) and high RH  
354 ( $63.6 \pm 27.1 \%$ ) favored the  $\text{ClNO}_2$  formation at Mt. Tai. The maximum level of  $\text{ClNO}_2$   
355 (approximately 1.7 ppbv) was observed just before midnight on 18 March, which was  
356 slightly lower than the highest concentration observed at Mt. Tai in the summer of 2014  
357 (Wang et al., 2017c). The elevated concentrations of  $\text{ClNO}_2$  observed in the previous  
358 summer study at Mt. Tai were due to emissions from distinct coal-fired power plants,  
359 whereas this winter study found that coal burning had less effect on concentrations of  
360  $\text{ClNO}_2$ . The campaign-averaged levels of  $\text{SO}_2$  and particulate  $\text{SO}_4^{2-}$  were  $1.6 \pm 1.6$  ppbv  
361 and  $3.6 \pm 2.9 \mu\text{g m}^{-3}$ , respectively, during the winter observations, which were  
362 significantly lower than those observed in the summer campaigns ( $2.9 \pm 3.7$  ppbv and  
363  $14.8 \pm 9.0 \mu\text{g m}^{-3}$ , respectively). The reduced effect from coal-fired power generation  
364 was due to the continued decrease in  $\text{SO}_2$  emissions during 2014–2018 and less transport  
365 of emissions from the ground to the Mt Tai site (1534 m a.s.l.) in late winter and early  
366 spring compared with that in summer.

367  
368 We compared the observed winter concentrations of  $\text{ClNO}_2$  with those reported in  
369 previous studies in Asia, North America, and Europe (Fig. 3). The highest winter  
370 concentrations of  $\text{ClNO}_2$  to date were observed in southern China, with a maximum  
371 level of 4.7 ppbv at a mountain top in Hong Kong in aged urban/industrial plumes from  
372 the Pearl River Delta (PRD) (Wang et al., 2016) and 8.3 ppbv during a severe pollution  
373 episode within the PRD (Yun et al., 2018). The high-concentration  $\text{ClNO}_2$  events in



374 southern China were due to concurrent high levels of  $\text{PM}_{2.5}$  and  $\text{O}_3$  (e.g.,  $400 \mu\text{g m}^{-3}$   
375 and 160 ppbv found by Yun et al., 2018), which contrasts the high concentrations of  
376  $\text{PM}_{2.5}$  and low concentrations of  $\text{O}_3$  over northern China during the cold winter. The  
377 winter mixing ratios of  $\text{ClNO}_2$  in the US and Europe range from approximately 0.3 ppbv  
378 in urban California (Mielke et al., 2016) and urban Manchester (Priestley et al., 2018),  
379 respectively, to 1.3 ppbv in the outflow of coastal urban areas (Riedel et al., 2013;  
380 Haskins et al., 2019). In general, the winter concentrations of  $\text{ClNO}_2$  over northern  
381 China were comparable to or slightly higher than those observed in the US and Europe.



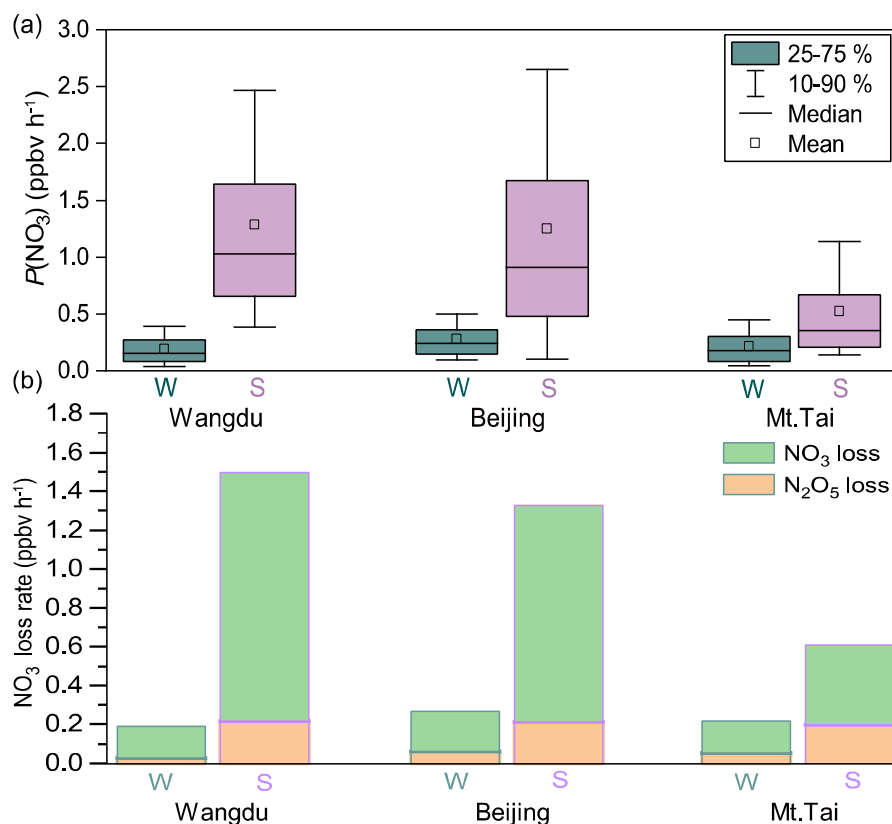
382 © Map.Ps123.Net  
383 Figure 3. Previous observations of  $\text{ClNO}_2$  and  $\text{N}_2\text{O}_5$  levels worldwide. Observation  
384 sites in this study are shown in bold. The  $\text{ClNO}_2$  and  $\text{N}_2\text{O}_5$  levels shown are the highest  
385 that were measured at these sites. Footnotes associated with the locations refer to the  
386 references as follows. 1. (Mielke et al., 2011; Mielke et al., 2016). 2. (Osthoff et al.,  
387 2008). 3. (Phillips et al., 2012). 4. (Tham et al., 2016; Liu et al., 2017). 5. (Wang et al.,  
388 2017a; Breton et al., 2018; Wang et al., 2018; Zhou et al., 2018; Xia et al., 2019). 6.  
389 (Nakayama et al., 2008). 7. (Wang et al., 2017c). 8. (Xia et al., 2020). 9. (Wang et al.,  
390 2019a). 10. (Wang et al., 2017b). 11. (Wang et al., 2016; Yun et al., 2017; Yan et al.,  
391 2019). 12. (Yun et al., 2018). 13. (Eger et al., 2019). 14. (Apodaca et al., 2008;  
392 McNamara et al., 2019). 15. (Thornton et al., 2010; Riedel et al., 2013). 16. (Riedel et  
393 al., 2012; Mielke et al., 2013). 17. (Brown et al., 2006; Brown et al., 2007). 18.  
394 (Crowley et al., 2011). 19. (Bannan et al., 2015). 20. (Bannan et al., 2019). 21. (Edwards  
395 et al., 2013; Wild et al., 2016).

### 396 397 3.2 $\text{NO}_3$ production and loss pathways

398 To gain insight into the processes controlling the variability in concentrations of  
399  $\text{ClNO}_2$ , nocturnal  $P(\text{NO}_3)$  and  $\text{NO}_3$  loss pathways were compared using Eqs. (1-5) in  
400 Section 2.4. The average  $P(\text{NO}_3)$  was comparable at the three sites in winter, ranging  
401 from  $0.15 \text{ ppbv h}^{-1}$  to  $0.25 \text{ ppbv h}^{-1}$ , and these rates were significantly lower than the  
402 respective summer values (Fig. 4a). The lower  $P(\text{NO}_3)$  in winter was caused by both  
403 lower  $k_1$  and lower  $[\text{NO}_2] \times [\text{O}_3]$  in winter (see Eq. 1). Nighttime  $\text{NO}_3$  removal through



404  $\text{NO}_3$  and  $\text{N}_2\text{O}_5$  was estimated by comparing  $k(\text{NO}_3) \times [\text{NO}_3]$  (Eqs. 2–3) and  $k(\text{N}_2\text{O}_5) \times$   
405  $[\text{N}_2\text{O}_5]$  (Eqs. 4–5). The average  $\gamma(\text{N}_2\text{O}_5)$  values derived from each campaign (Table S4  
406 and Fig. S8) were used in Eq. (4). The nighttime  $\text{NO}_3$  loss via NO titration and VOC  
407 oxidation was greater than the  $\text{N}_2\text{O}_5$  heterogeneous loss in all the winter and summer  
408 campaigns (Fig. 4b). These were the campaign average results. In contrast, the  $\text{N}_2\text{O}_5$   
409 loss was greater than the  $\text{NO}_3$  loss in selected cases in summer at Mt. Tai (Wang et al.,  
410 2017c). To determine the nocturnal loss of  $\text{NO}_3$ , we further compared the  $\text{N}_2\text{O}_5/\text{NO}_3$   
411 ratio and  $\gamma(\text{N}_2\text{O}_5)$  at the three sites.  
412

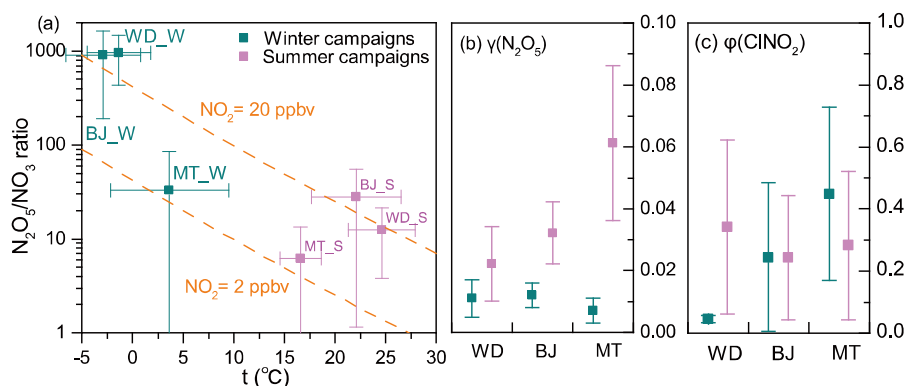


413  
414 **Figure 4.** Comparison of  $P(\text{NO}_3)$  and loss pathways of  $\text{NO}_3$  during the winter and  
415 summer observations over the NCP. W and S are abbreviations for winter and summer,  
416 respectively.

417  
418 The thermal decomposition of  $\text{N}_2\text{O}_5$  was suppressed in winter and resulted in high  
419 ratios of  $\text{N}_2\text{O}_5/\text{NO}_3$  (Fig. 5a; up to approximately 1000), which favored  $\text{N}_2\text{O}_5$  loss over  
420  $\text{NO}_3$  loss. However, the  $\gamma(\text{N}_2\text{O}_5)$  in winter was systematically lower than that in summer  
421 (Fig. 5b), which indicated slower  $\text{N}_2\text{O}_5$  loss in winter. This result differs from previous  
422 laboratory studies, which reported larger  $\gamma(\text{N}_2\text{O}_5)$  on  $(\text{NH}_4)_2\text{SO}_4$  aerosols at lower  
423 temperatures (Hallquist et al., 2003; Griffiths and Anthony Cox, 2009). It is possible



424 that other factors, such as RH and aerosol composition (aside from  $(\text{NH}_4)_2\text{SO}_4$ ), had a  
425 large influence on  $\gamma(\text{N}_2\text{O}_5)$ . The limited number (2–4) of  $\gamma(\text{N}_2\text{O}_5)$  values obtained in  
426 each winter campaign (Table S4) may have also caused a bias in the estimation of the  
427 overall  $\gamma(\text{N}_2\text{O}_5)$ . The opposite effects – a higher  $\text{N}_2\text{O}_5/\text{NO}_3$  ratio and lower  $\gamma(\text{N}_2\text{O}_5)$  in  
428 winter – offset each other in Wangdu (Fig. 4b) but favored  $\text{N}_2\text{O}_5$  loss in Beijing and  
429  $\text{NO}_3$  loss at Mt. Tai compared with those in the respective summer campaigns. The  
430 higher concentrations of  $\text{ClNO}_2$  at Mt. Tai during the winter campaigns may be  
431 attributable to higher  $\phi(\text{ClNO}_2)$  values in Mt. Tai (Fig. 5c).  
432



433  
434 **Figure 5.** Comparison of the (a)  $\text{N}_2\text{O}_5/\text{NO}_3$  ratio, (b)  $\gamma(\text{N}_2\text{O}_5)$ , and (c)  $\phi(\text{ClNO}_2)$  during  
435 the winter and summer campaigns. Square dots and error bars indicate the average  
436 values and standard deviations, respectively.

### 437 3.3 Daytime peaks in $\text{ClNO}_2$ concentrations

438 In the winter campaigns, high concentrations of  $\text{ClNO}_2$  were sustained after sunrise.  
439 Distinct peaks in  $\text{ClNO}_2$  concentrations were observed on 3–4 days in each campaign,  
440 as shown in Fig. 6. Other daytime cases from the three sites are shown in Fig. S9–11.  
441 The validity of the daytime peaks was checked by performing isotopic analysis of  
442  $\text{ClNO}_2$ , background detection, and onsite calibration. The signals of  $\text{I}^{35}\text{ClNO}_2^-$  and  
443  $\text{I}^{37}\text{ClNO}_2^-$  were well correlated ( $R^2 > 0.99$ ) during daytime peaks in  $\text{ClNO}_2$   
444 concentrations (Fig. S3a–c) and calibrations (Fig. S3d–f). The ratio of  $\text{I}^{37}\text{ClNO}_2^-$  to  
445  $\text{I}^{35}\text{ClNO}_2^-$  (0.32–0.35) was consistent with the natural isotopic ratio of  $^{37}\text{Cl}$  to  $^{35}\text{Cl}$ . The  
446 background signals of  $\text{ClNO}_2$  were checked when its daytime peaks in concentrations  
447 were observed, and no increase in the background was found. These results confirmed  
448 that the daytime peaks in  $\text{ClNO}_2$  concentrations were real atmospheric phenomena.  
449

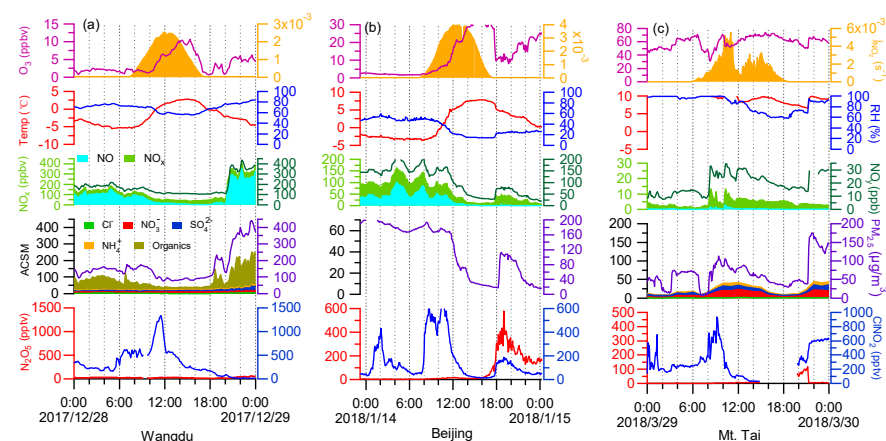
450  
451 The daytime- $\text{ClNO}_2$  episodes usually occurred from 10:00 to 11:00 LT at each site.  
452 The highest daytime mixing ratio of  $\text{ClNO}_2$  was 1.3 ppbv (5-minute average) observed  
453 at 11:30 on 28 December 2017 in Wangdu. In comparison, the daytime  $\text{ClNO}_2$   
454 concentration observed in the previous summer study at Wangdu (Tham et al., 2016)  
455 reached a maximum in the early morning (08:00 LT) and declined to several pptv at  
456 11:00 am. Attenuated solar radiation was observed during the days with daytime peaks



457 in CINO<sub>2</sub> concentrations. For example, the daily maximum rates of  $j\text{NO}_2$  (1-minute  
458 average) for the Wangdu case shown in Fig. 6a ( $2.5 \times 10^{-3} \text{ s}^{-1}$ ) was significantly lower  
459 than the highest rate observed during this campaign ( $6.0 \times 10^{-3} \text{ s}^{-1}$ ). The attenuated solar  
460 radiation reduced the photolysis of CINO<sub>2</sub>, which allowed it to persist for a longer  
461 period during the day. The chemical data showed contrasting features during the  
462 daytime peaks in CINO<sub>2</sub> concentrations at the three sites. At Wangdu, CINO<sub>2</sub>  
463 concentrations showed a sharp peak while the concentrations of other pollutants  
464 decreased (Fig. 6a); in Beijing, the daytime peak in CINO<sub>2</sub> concentrations appeared  
465 with little simultaneous change in the NO<sub>3</sub><sup>-</sup>, NO<sub>x</sub>, and O<sub>3</sub> levels after sunrise (Fig. S10a).  
466 In two cases, daytime peaks of CINO<sub>2</sub> concentrations at Mt. Tai (Fig. 6c and Fig. S11c)  
467 occurred together with significant increases in NO<sub>3</sub><sup>-</sup>, NO<sub>x</sub>, and PM<sub>2.5</sub> levels, whereas  
468 O<sub>3</sub> concentrations decreased after sunrise and resumed its previous levels.

469 The daytime peaks in CINO<sub>2</sub> concentrations were likely caused by the transport of  
470 air masses to the respective sites. In situ production of CINO<sub>2</sub> was limited during the  
471 days on which significant daytime CINO<sub>2</sub> occurred, because the mixing ratios of N<sub>2</sub>O<sub>5</sub>  
472 were near the detection limit of the instrument (several pptv). The photochemical  
473 lifetime of CINO<sub>2</sub> at 10:00 am LT was estimated to be 1–2 h, based on the inverse of  
474  $j\text{CINO}_2$ , which allowed the transport of CINO<sub>2</sub> produced elsewhere to the observation  
475 sites. As daytime peaks in CINO<sub>2</sub> concentrations appeared at both the ground and  
476 mountain sites, the high-CINO<sub>2</sub> region may exist in the residual layer above the  
477 nocturnal mixing layers. At sunrise, CINO<sub>2</sub>-rich air masses may be transported  
478 downward to the ground sites (Wangdu and Beijing) and upward to the mountain-top  
479 site (Mt. Tai). The downward transport of CINO<sub>2</sub> at Wangdu in summer has been  
480 illustrated by Tham et al. (2016), and the upward transport to the top of Mt. Tai has also  
481 been implicated by the increasing daytime concentrations of O<sub>3</sub> and other pollutants  
482 (e.g., Gao et al., 2005; Zhou et al., 2009; Jiang et al., 2020). Measurements in the  
483 residual layers are needed to further investigate the transport of CINO<sub>2</sub> within the entire  
484 boundary layer.

485



486  
487 **Figure 6.** Examples of daytime peaks of CINO<sub>2</sub> levels observed at (a) Wangdu, (b)  
488 Beijing, and (c) Mt. Tai in the winter campaigns. These examples show the highest



489 levels of daytime ClNO<sub>2</sub> at each site. The ionic composition of aerosols was not  
490 available on 14 January 2018, owing to an instrument problem.

491

### 492 3.4 Impact of daytime ClNO<sub>2</sub> on atmospheric oxidation capacity

493 We used the box model (Section 2.5) to show the impact of ClNO<sub>2</sub> on photochemical  
494 oxidation at the three sites (Fig. 6a–c). In campaign-averaged conditions, the impact of  
495 ClNO<sub>2</sub> was minor, owing to the low daytime concentrations of ClNO<sub>2</sub>. The daytime-  
496 averaged  $P(\text{Cl})$  (06:00–18:00 LT) from ClNO<sub>2</sub> photolysis was in the range of 0.03–0.06  
497 ppbv h<sup>-1</sup>, with the peak values of 0.07–0.12 ppbv h<sup>-1</sup>, and the photolysis of ClNO<sub>2</sub>  
498 enhanced the daytime RO<sub>x</sub> concentrations by 1.3–3.8 % and net O<sub>3</sub> production by 1.3–  
499 6.2 % at the three sites (figures not shown). Such impacts were lower than those during  
500 summer at Wangdu (Tham et al., 2016).

501

502 However, the impact of ClNO<sub>2</sub> increased considerably in the cases of daytime-peak  
503 concentrations, as shown in Fig. 7. The daytime-averaged  $P(\text{Cl})$  values from ClNO<sub>2</sub>  
504 photolysis were  $0.15 \pm 0.13$  (maximum of 0.46),  $0.11 \pm 0.09$  (maximum of 0.32), and  
505  $0.19 \pm 0.20$  (maximum of 0.74) ppbv h<sup>-1</sup> at Wangdu, Beijing, and Mt. Tai, respectively  
506 (Fig. 7a–c). The winter  $P(\text{Cl})$  peak in Wangdu (Fig. 7a, 0.46 ppbv h<sup>-1</sup>) was twice the  
507 summer average value (0.24 ppbv h<sup>-1</sup>) (Tham et al., 2016).  $P(\text{Cl})$  from other sources  
508 (e.g., the HCl + OH reaction) was minor (8.8–14.5 %) during these cases. The relative  
509 importance of ClNO<sub>2</sub> in primary radical production varied among these sites. ClNO<sub>2</sub>  
510 had a minor contribution in Beijing but became increasingly important in Wangdu and  
511 Mt. Tai (Fig. 7b, c). HONO photolysis was the most important source of OH at the two  
512 ground sites, whereas O<sub>3</sub> was also important at Mt. Tai.

513

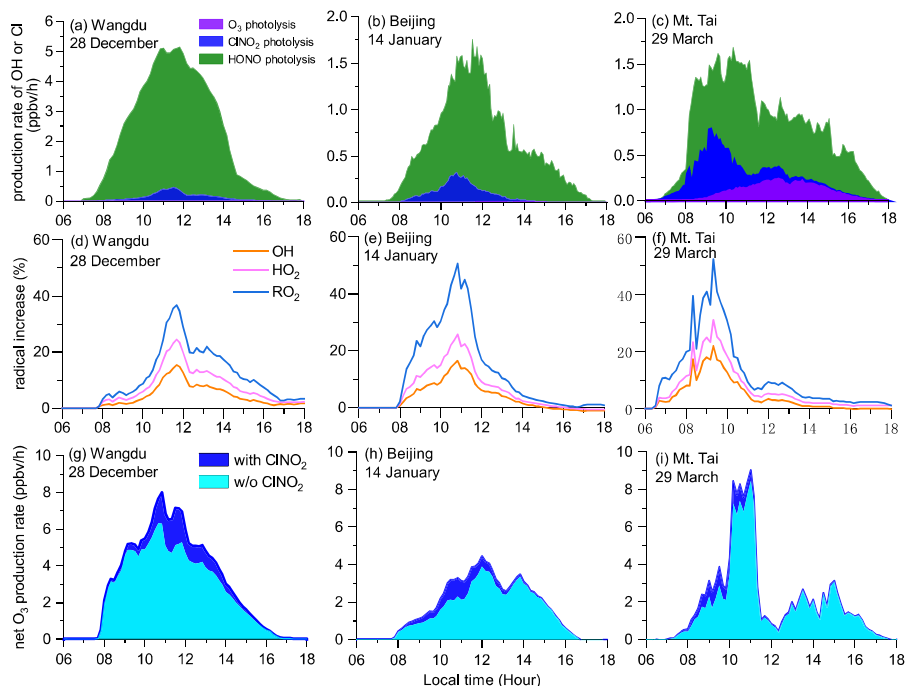
514 The liberated Cl (mostly from ClNO<sub>2</sub> photolysis) accounted for 28.5–57.7 % of the  
515 daytime (06:00–18:00 LT) oxidation of alkanes, 6.1–13.7 % of that of alkenes, 5.3–  
516 14.2 % of that of aromatics, and 4.6–6.0 % of that of aldehydes in the cases of high  
517 levels of daytime ClNO<sub>2</sub>. The Cl + VOCs reactions enhanced the production of OH,  
518 HO<sub>2</sub>, and RO<sub>2</sub> by up to 15–22 %, 24–31 %, and 36–52 %, respectively (Fig. 7d–f). The  
519 photolysis of ClNO<sub>2</sub> increased the daytime net O<sub>3</sub> production by 5.4 ppbv (18 %), 2.8  
520 ppbv (17 %), and 2.6 ppbv (13%) at Wangdu, Beijing, and Mt. Tai, respectively (Fig.  
521 7g–i). These results indicate the considerable impact of daytime ClNO<sub>2</sub> on the  
522 atmospheric oxidative capacity and production of secondary pollutants.

523

524 The impact of Cl in the NCP is likely larger than the result shown above. Our model  
525 calculations considered photolysis of ClNO<sub>2</sub> (and HCl + OH) as the source of Cl, but  
526 not other photolabile Cl-containing gases. However, in the Wangdu field campaign, we  
527 frequently observed elevated daytime concentrations of bromine chloride (BrCl) and  
528 molecular chlorine (Cl<sub>2</sub>), which dominated the Cl production (Peng et al., 2020). In  
529 addition, our ClNO<sub>2</sub> measurements were conducted at polluted ground-level sites and  
530 at a high mountain site (1534 m a.s.l.), which are not in the nocturnal residual layer  
531 where strong ClNO<sub>2</sub> production is expected to occur (Zhang et al., 2017). It is thus  
532 highly desirable to measure ClNO<sub>2</sub> in the residual layer in future studies to



533 comprehensively assess the role of CINO<sub>2</sub> in the lower part of the atmosphere.



534

535 **Figure 7.** The impact of CINO<sub>2</sub> photolysis on atmospheric oxidation during daytime-  
536 CINO<sub>2</sub> episodes: (a) primary radical production from the photolysis of O<sub>3</sub>, CINO<sub>2</sub>, and  
537 HONO; (b) percentage increase in OH, HO<sub>2</sub>, and RO<sub>2</sub> due to CINO<sub>2</sub> photolysis (Section  
538 2.5); and (c) enhancement of net O<sub>3</sub> production rates due to CINO<sub>2</sub> photolysis.

539

#### 540 4. Summary and conclusions

541 Observations of CINO<sub>2</sub> and related species were conducted at urban, rural, and  
542 mountain-top sites in the winter of 2017–2018 in the NCP, which suffers from severe  
543 winter haze pollution. The winter measurements showed lower concentrations of  
544 CINO<sub>2</sub> compared with those in previous summer observations. The campaign averaged  
545 NO<sub>3</sub> loss at night dominated over the N<sub>2</sub>O<sub>5</sub> loss at all the sites due to high NO  
546 concentrations, and in situ CINO<sub>2</sub> formation was generally insignificant. However, high  
547 levels of daytime CINO<sub>2</sub> (exceeding 1 ppbv) were observed at the three sites. We  
548 suggest that CINO<sub>2</sub> was efficiently produced in the nocturnal residual layer and was  
549 transported to ground-level and high-elevation sites. The daytime concentrations of  
550 CINO<sub>2</sub> had great effects on the production of Cl, RO<sub>x</sub>, and O<sub>3</sub>. Vertical measurements  
551 of the concentrations of CINO<sub>2</sub> and related compounds are needed to better understand  
552 the distribution and impact of these species in the lower part of the troposphere.

553

#### 554 Data availability.

555 The datasets described in this study is available by contacting the corresponding  
556 author (cetwang@polyu.edu.hk).





557

558 *Author contributions.*

559 TW designed this study. JC, YM, LX, JG, and HL provided field measurement sites.  
560 MX, XP, and WW conducted the CIMS measurements. CY, ZW, YJT, HC, CZ, PL, and  
561 XW provided supporting data. XP and WW performed the box model simulation. MX  
562 analyzed and virtualized the research data. MX and TW wrote the manuscript with  
563 discussions and comments from all co-authors.

564

565 *Competing interests.*

566 The authors declare that they have no conflict of interest.

567

568 *Acknowledgments.*

569 The authors are grateful to Yujie Zhang, Fang Bi, Zhenhai Wu, and Xi Cheng for  
570 providing supporting data in Beijing. The authors acknowledge helpful discussions and  
571 opinions from Peng Wang, Xiao Fu, logistics support from Liwei Guan in Wangdu, and  
572 the meteorological observatory at Mt. Tai for providing experiment platforms.

573

574 *Financial support.*

575 This work was funded by National Natural Science Foundation of China (grant nos.  
576 91544213, 91844301, and 41922051), the Hong Kong Research Grants Council (grant  
577 nos. T24-504/17-N and A-PolyU502/16), and National Key Research and Development  
578 Program of China (grant no. 2016YFC0200500).

579

## 580 **References**

581 Achtert, P., Birmili, W., Nowak, A., Wehner, B., Wiedensohler, A., Takegawa, N.,  
582 Kondo, Y., Miyazaki, Y., Hu, M., and Zhu, T.: Hygroscopic growth of tropospheric  
583 particle number size distributions over the North China Plain, *Journal of Geophysical*  
584 *Research: Atmospheres*, 114, D00G07, 2009.

585 An, Z., Huang, R.-J., Zhang, R., Tie, X., Li, G., Cao, J., Zhou, W., Shi, Z., Han, Y., Gu,  
586 Z., and Ji, Y.: Severe haze in northern China: A synergy of anthropogenic emissions and  
587 atmospheric processes, *Proceedings of the National Academy of Sciences*, 116, 8657-  
588 8666, 10.1073/pnas.1900125116, 2019.

589 Apodaca, R., Huff, D., and Simpson, W.: The role of ice in N<sub>2</sub>O<sub>5</sub> heterogeneous  
590 hydrolysis at high latitudes, *Atmospheric Chemistry and Physics*, 8, 7451-7463, 2008.

591 Atkinson, R., and Arey, J.: Atmospheric degradation of volatile organic compounds,  
592 *Chemical reviews*, 103, 4605-4638, 2003.

593 Bannan, T. J., Booth, A. M., Bacak, A., Muller, J. B. A., Leather, K. E., Le Breton, M.,  
594 Jones, B., Young, D., Coe, H., Allan, J., Visser, S., Slowik, J. G., Furger, M., Prévôt, A.  
595 S. H., Lee, J., Dunmore, R. E., Hopkins, J. R., Hamilton, J. F., Lewis, A. C., Whalley,  
596 L. K., Sharp, T., Stone, D., Heard, D. E., Fleming, Z. L., Leigh, R., Shallcross, D. E.,  
597 and Percival, C. J.: The first UK measurements of nitryl chloride using a chemical  
598 ionization mass spectrometer in central London in the summer of 2012, and an  
599 investigation of the role of Cl atom oxidation, *Journal of Geophysical Research:*  
600 *Atmospheres*, 120, 5638-5657, 10.1002/2014jd022629, 2015.



- 601 Bannan, T. J., Khan, M. A. H., Le Breton, M., Priestley, M., Worrall, S. D., Bacak, A.,  
602 Marsden, N. A., Lowe, D., Pitt, J., and Allen, G.: A large source of atomic chlorine from  
603 ClNO<sub>2</sub> photolysis at a UK landfill site, *Geophysical Research Letters*, 46, 8508-8516,  
604 2019.
- 605 Behnke, W., George, C., Scheer, V., and Zetzsch, C.: Production and decay of ClNO<sub>2</sub>  
606 from the reaction of gaseous N<sub>2</sub>O<sub>5</sub> with NaCl solution: Bulk and aerosol experiments,  
607 *Journal of Geophysical Research: Atmospheres*, 102, 3795-3804, 1997.
- 608 Bertram, T., and Thornton, J.: Toward a general parameterization of N<sub>2</sub>O<sub>5</sub> reactivity on  
609 aqueous particles: the competing effects of particle liquid water, nitrate and chloride,  
610 *Atmospheric Chemistry and Physics*, 9, 8351-8363, 2009.
- 611 Bertram, T. H., Thornton, J. A., Riedel, T. P., Middlebrook, A. M., Bahreini, R., Bates,  
612 T. S., Quinn, P. K., and Coffman, D. J.: Direct observations of N<sub>2</sub>O<sub>5</sub> reactivity on  
613 ambient aerosol particles, *Geophysical Research Letters*, 36, L19803, 2009.
- 614 Breton, M. L., Hallquist, Å. M., Pathak, R. K., Simpson, D., Wang, Y., Johansson, J.,  
615 Zheng, J., Yang, Y., Shang, D., and Wang, H.: Chlorine oxidation of VOCs at a semi-  
616 rural site in Beijing: significant chlorine liberation from ClNO<sub>2</sub> and subsequent gas-and  
617 particle-phase Cl-VOC production, *Atmospheric Chemistry and Physics*, 18, 13013-  
618 13030, 2018.
- 619 Brown, S., Ryerson, T., Wollny, A., Brock, C., Peltier, R., Sullivan, A., Weber, R., Dube,  
620 W., Trainer, M., and Meagher, J.: Variability in nocturnal nitrogen oxide processing and  
621 its role in regional air quality, *Science*, 311, 67-70, 2006.
- 622 Brown, S. S., Stark, H., Ryerson, T. B., Williams, E. J., Nicks, D. K., Trainer, M.,  
623 Fehsenfeld, F. C., and Ravishankara, A.: Nitrogen oxides in the nocturnal boundary  
624 layer: Simultaneous in situ measurements of NO<sub>3</sub>, N<sub>2</sub>O<sub>5</sub>, NO<sub>2</sub>, NO, and O<sub>3</sub>, *Journal of*  
625 *Geophysical Research: Atmospheres*, 108, 4299, 2003.
- 626 Brown, S. S., Dubé, W. P., Osthoff, H. D., Stutz, J., Ryerson, T. B., Wollny, A. G., Brock,  
627 C. A., Warneke, C., De Gouw, J. A., and Atlas, E.: Vertical profiles in NO<sub>3</sub> and N<sub>2</sub>O<sub>5</sub>  
628 measured from an aircraft: Results from the NOAA P-3 and surface platforms during  
629 the New England Air Quality Study 2004, *Journal of Geophysical Research:*  
630 *Atmospheres*, 112, D22304, 2007.
- 631 Burkholder, J., Sander, S., Abbatt, J., Barker, J., Huie, R., Kolb, C., Kurylo, M., Orkin,  
632 V., Wilmouth, D., and Wine, P.: Chemical kinetics and photochemical data for use in  
633 atmospheric studies: evaluation number 18, Pasadena, CA: Jet Propulsion Laboratory,  
634 National Aeronautics and Space, 2015.
- 635 Chang, W. L., Bhave, P. V., Brown, S. S., Riemer, N., Stutz, J., and Dabdub, D.:  
636 Heterogeneous atmospheric chemistry, ambient measurements, and model calculations  
637 of N<sub>2</sub>O<sub>5</sub>: A review, *Aerosol Science and Technology*, 45, 665-695, 2011.
- 638 Crowley, J., Thieser, J., Tang, M., Schuster, G., Bozem, H., Beygi, Z. H., Fischer, H.,  
639 Diesch, J., Drewnick, F., and Borrmann, S.: Variable lifetimes and loss mechanisms for  
640 NO<sub>3</sub> and N<sub>2</sub>O<sub>5</sub> during the DOMINO campaign: contrasts between marine, urban and  
641 continental air, *Atmospheric Chemistry and Physics*, 11, 10853-10870, 2011.
- 642 Edwards, P. M., Young, C. J., Aikin, K., deGouw, J., Dubé, W. P., Geiger, F., Gilman,  
643 J., Helmig, D., Holloway, J. S., Kercher, J., Lerner, B., Martin, R., McLaren, R., Parrish,  
644 D. D., Peischl, J., Roberts, J. M., Ryerson, T. B., Thornton, J., Warneke, C., Williams,



- 645 E. J., and Brown, S. S.: Ozone photochemistry in an oil and natural gas extraction region  
646 during winter: simulations of a snow-free season in the Uintah Basin, Utah, *Atmos.*  
647 *Chem. Phys.*, 13, 8955–8971, <https://doi.org/10.5194/acp-13-8955-2013>, 2013.
- 648 Eger, P., Friedrich, N., Schuladen, J., Shenolikar, J., Fischer, H., Tadic, I., Harder, H.,  
649 Martinez, M., Rohloff, R., Tauer, S., Drewnick, F., Fachinger, F., Brooks, J., Darbyshire,  
650 E., Sciare, J., Pikridas, M., Lelieveld, J., and Crowley, J.: Shipborne measurements of  
651 CINO<sub>2</sub> in the Mediterranean Sea and around the Arabian Peninsula during summer,  
652 *Atmospheric Chemistry and Physics*, 19, 12121–12140, [10.5194/acp-19-12121-2019](https://doi.org/10.5194/acp-19-12121-2019),  
653 2019.
- 654 Finlayson-Pitts, B., Ezell, M., and Pitts, J.: Formation of chemically active chlorine  
655 compounds by reactions of atmospheric NaCl particles with gaseous N<sub>2</sub>O<sub>5</sub> and ClONO<sub>2</sub>,  
656 *Nature*, 337, 241–244, 1989.
- 657 Fu, X., Wang, T., Wang, S., Zhang, L., Cai, S., Xing, J., and Hao, J.: Anthropogenic  
658 emissions of hydrogen chloride and fine particulate chloride in China, *Environmental*  
659 *Science & Technology*, 52, 1644–1654, 2018.
- 660 Fu, X., Wang, T., Gao, J., Wang, P., Liu, Y., Wang, S., Zhao, B., and Xue, L.: Persistent  
661 Heavy Winter Nitrate Pollution Driven by Increased Photochemical Oxidants in  
662 Northern China, *Environmental Science & Technology*, 54, 3881–3889, 2020.
- 663 Gao, J., Wang, T., Ding, A., and Liu, C.: Observational study of ozone and carbon  
664 monoxide at the summit of mount Tai (1534 m asl) in central-eastern China,  
665 *Atmospheric Environment*, 39, 4779–4791, 2005.
- 666 Griffiths, P. T., and Anthony Cox, R.: Temperature dependence of heterogeneous uptake  
667 of N<sub>2</sub>O<sub>5</sub> by ammonium sulfate aerosol, *Atmospheric Science Letters*, 10, 159–163,  
668 [10.1002/asl.225](https://doi.org/10.1002/asl.225), 2009.
- 669 Hallquist, M., Stewart, D. J., Stephenson, S. K., and Cox, R. A.: Hydrolysis of N<sub>2</sub>O<sub>5</sub> on  
670 sub-micron sulfate aerosols, *Physical Chemistry Chemical Physics*, 5, 3453–3463, 2003.
- 671 Haskins, J., Lopez-Hilfiker, F., Lee, B., Shah, V., Wolfe, G., DiGangi, J., Fibiger, D.,  
672 McDuffie, E., Veres, P., and Schroder, J.: Anthropogenic control over wintertime  
673 oxidation of atmospheric pollutants, *Geophysical Research Letters*, 46, 14826–14835,  
674 2019.
- 675 Jenkin, M., Young, J., and Rickard, A.: The MCM v3. 3.1 degradation scheme for  
676 isoprene, *Atmospheric Chemistry and Physics*, 15, 11433, 2015.
- 677 Lewis, E. R.: An examination of Köhler theory resulting in an accurate expression for  
678 the equilibrium radius ratio of a hygroscopic aerosol particle valid up to and including  
679 relative humidity 100%, *Journal of Geophysical Research: Atmospheres*, 113, D03205,  
680 2008.
- 681 Liu, X., Qu, H., Huey, L. G., Wang, Y., Sjostedt, S., Zeng, L., Lu, K., Wu, Y., Hu, M.,  
682 and Shao, M.: High levels of daytime molecular chlorine and nitryl chloride at a rural  
683 site on the North China Plain, *Environmental science & technology*, 51, 9588–9595,  
684 2017.
- 685 McCulloch, A., Aucott, M. L., Benkovitz, C. M., Graedel, T. E., Kleiman, G., Midgley,  
686 P. M., and Li, Y. F.: Global emissions of hydrogen chloride and chloromethane from  
687 coal combustion, incineration and industrial activities: Reactive Chlorine Emissions  
688 Inventory, *Journal of Geophysical Research: Atmospheres*, 104, 8391–8403, 1999.



- 689 McNamara, S. M., Raso, A. R., Wang, S., Thanekar, S., Boone, E. J., Kolesar, K. R.,  
690 Peterson, P. K., Simpson, W. R., Fuentes, J. D., and Shepson, P. B.: Springtime Nitrogen  
691 Oxide-Influenced Chlorine Chemistry in the Coastal Arctic, *Environmental science &*  
692 *technology*, 53, 8057-8067, 2019.
- 693 Mielke, L., Stutz, J., Tsai, C., Hurlock, S., Roberts, J., Veres, P., Froyd, K., Hayes, P.,  
694 Cubison, M., and Jimenez, J.: Heterogeneous formation of nitryl chloride and its role  
695 as a nocturnal NO<sub>x</sub> reservoir species during CalNex-LA 2010, *Journal of Geophysical*  
696 *Research: Atmospheres*, 118, 10638-10652, 2013.
- 697 Mielke, L. H., Furgeson, A., and Osthoff, H. D.: Observation of ClNO<sub>2</sub> in a mid-  
698 continental urban environment, *Environmental Science & Technology*, 45, 8889-8896,  
699 10.1021/es201955u, 2011.
- 700 Mielke, L. H., Furgeson, A., Odame-Ankrah, C. A., and Osthoff, H. D.: Ubiquity of  
701 ClNO<sub>2</sub> in the urban boundary layer of Calgary, Alberta, Canada, *Canadian Journal of*  
702 *Chemistry*, 94, 414-423, 2016.
- 703 Molina, M. J., and Rowland, F. S.: Stratospheric sink for chlorofluoromethanes:  
704 chlorine atom-catalysed destruction of ozone, *Nature*, 249, 810-812, 1974.
- 705 Nakayama, T., Ide, T., Taketani, F., Kawai, M., Takahashi, K., and Matsumi, Y.:  
706 Nighttime measurements of ambient N<sub>2</sub>O<sub>5</sub>, NO<sub>2</sub>, NO and O<sub>3</sub> in a sub-urban area,  
707 Toyokawa, Japan, *Atmospheric Environment*, 42, 1995-2006, 2008.
- 708 Osthoff, H. D., Roberts, J. M., Ravishankara, A. R., Williams, E. J., Lerner, B. M.,  
709 Sommariva, R., Bates, T. S., Coffman, D., Quinn, P. K., Dibb, J. E., Stark, H.,  
710 Burkholder, J. B., Talukdar, R. K., Meagher, J., Fehsenfeld, F. C., and Brown, S. S.:  
711 High levels of nitryl chloride in the polluted subtropical marine boundary layer, *Nature*  
712 *Geoscience*, 1, 324-328, 10.1038/ngeo177, 2008.
- 713 Peng, X., Wang, M. Xia, H. Chen, A. R. Ravishankara, Q. Li, A. Saiz-Lopez, P. Liu,  
714 F. Zhang, C. Zhang, L. Xue, X. Wang, C. George, J. Wang, Y. Mu, J. Chen, and T. Wang,  
715 An unexpected large continental source of reactive bromine and chlorine with  
716 significant impact on wintertime air quality, *National Science Review*,  
717 <https://doi.org/10.1093/nsr/nwaa304>, 2020
- 718 Phillips, G. J., Tang, M. J., Thieser, J., Brickwedde, B., Schuster, G., Bohn, B.,  
719 Lelieveld, J., and Crowley, J. N.: Significant concentrations of nitryl chloride observed  
720 in rural continental Europe associated with the influence of sea salt chloride and  
721 anthropogenic emissions, *Geophysical Research Letters*, 39, L10811,  
722 10.1029/2012gl051912, 2012.
- 723 Phillips, G. J., Thieser, J., Tang, M., Sobanski, N., Schuster, G., Fachinger, J., Drewnick,  
724 F., Borrmann, S., Bingemer, H., and Lelieveld, J.: Estimating N<sub>2</sub>O<sub>5</sub> uptake coefficients  
725 using ambient measurements of NO<sub>3</sub>, N<sub>2</sub>O<sub>5</sub>, ClNO<sub>2</sub> and particle-phase nitrate,  
726 *Atmospheric Chemistry and Physics*, 16, 13231-13249, 2016.
- 727 Priestley, M., Breton, M. I., Bannan, T. J., Worrall, S. D., Bacak, A., Smedley, A. R.,  
728 Reyes-Villegas, E., Mehra, A., Allan, J., and Webb, A. R.: Observations of organic and  
729 inorganic chlorinated compounds and their contribution to chlorine radical  
730 concentrations in an urban environment in northern Europe during the wintertime,  
731 *Atmospheric Chemistry and Physics*, 18, 13481-13493, 2018.
- 732 Riedel, T., Wolfe, G., Danas, K., Gilman, J., Kuster, W., Bon, D., Vlasenko, A., Li, S.-



- 733 M., Williams, E., and Lerner, B.: An MCM modeling study of nitryl chloride (CINO<sub>2</sub>)  
734 impacts on oxidation, ozone production and nitrogen oxide partitioning in polluted  
735 continental outflow, *Atmospheric Chemistry and Physics*, 14, 3789-3800, 2014.
- 736 Riedel, T. P., Bertram, T. H., Crisp, T. A., Williams, E. J., Lerner, B. M., Vlasenko, A.,  
737 Li, S. M., Gilman, J., de Gouw, J., Bon, D. M., Wagner, N. L., Brown, S. S., and  
738 Thornton, J. A.: Nitryl chloride and molecular chlorine in the coastal marine boundary  
739 layer, *Environmental Science & Technology*, 46, 10463-10470, 10.1021/es204632r,  
740 2012.
- 741 Riedel, T. P., Wagner, N. L., Dubé, W. P., Middlebrook, A. M., Young, C. J., Öztürk, F.,  
742 Bahreini, R., VandenBoer, T. C., Wolfe, D. E., and Williams, E. J.: Chlorine activation  
743 within urban or power plant plumes: Vertically resolved CINO<sub>2</sub> and Cl<sub>2</sub> measurements  
744 from a tall tower in a polluted continental setting, *Journal of Geophysical Research: Atmospheres*, 118, 8702-8715, 2013.
- 746 Sandu, A., and Sander, R.: Simulating chemical systems in Fortran90 and Matlab with  
747 the Kinetic PreProcessor KPP-2.1, *Atmospheric Chemistry and Physics*, 6, 187-195,  
748 2006.
- 749 Tan, Z., Fuchs, H., Lu, K., Hofzumahaus, A., Bohn, B., Broch, S., Dong, H., Gomm, S.,  
750 Häsel, R., and He, L.: Radical chemistry at a rural site (Wangdu) in the North China  
751 Plain: observation and model calculations of OH, HO<sub>2</sub> and RO<sub>2</sub> radicals, *Atmospheric  
752 Chemistry and Physics*, 17, 663-690, 2017.
- 753 Tham, Y. J., Wang, Z., Li, Q., Yun, H., Wang, W., Wang, X., Xue, L., Lu, K., Ma, N.,  
754 Bohn, B., Li, X., Kecorius, S., Größ, J., Shao, M., Wiedensohler, A., Zhang, Y., and  
755 Wang, T.: Significant concentrations of nitryl chloride sustained in the morning:  
756 investigations of the causes and impacts on ozone production in a polluted region of  
757 northern China, *Atmospheric Chemistry and Physics*, 16, 14959-14977, 10.5194/acp-  
758 16-14959-2016, 2016.
- 759 Thornton, J. A., Kercher, J. P., Riedel, T. P., Wagner, N. L., Cozic, J., Holloway, J. S.,  
760 Dube, W. P., Wolfe, G. M., Quinn, P. K., Middlebrook, A. M., Alexander, B., and Brown,  
761 S. S.: A large atomic chlorine source inferred from mid-continental reactive nitrogen  
762 chemistry, *Nature*, 464, 271-274, 10.1038/nature08905, 2010.
- 763 Wang, H., Lu, K., Chen, X., Zhu, Q., Chen, Q., Guo, S., Jiang, M., Li, X., Shang, D.,  
764 and Tan, Z.: High N<sub>2</sub>O<sub>5</sub> Concentrations Observed in Urban Beijing: Implications of a  
765 Large Nitrate Formation Pathway, *Environmental Science & Technology Letters*, 2017a.
- 766 Wang, H., Lu, K., Guo, S., Wu, Z., Shang, D., Tan, Z., Wang, Y., Breton, M. L., Zhu,  
767 W., and Lou, S.: Efficient N<sub>2</sub>O<sub>5</sub> Uptake and NO<sub>3</sub> Oxidation in the Outflow of Urban  
768 Beijing, *Atmospheric Chemistry and Physics*, 18, 9705-9721, 2018.
- 769 Wang, H., Chen, X., Lu, K., Hu, R., Li, Z., Wang, H., Ma, X., Yang, X., Chen, S., and  
770 Dong, H.: NO<sub>3</sub> and N<sub>2</sub>O<sub>5</sub> chemistry at a suburban site during the EXPLORE-YRD  
771 campaign in 2018, *Atmospheric Environment*, 224, 117180, 2019a.
- 772 Wang, T., Tham, Y. J., Xue, L., Li, Q., Zha, Q., Wang, Z., Poon, S. C., Dubé, W. P.,  
773 Blake, D. R., and Louie, P. K.: Observations of nitryl chloride and modeling its source  
774 and effect on ozone in the planetary boundary layer of southern China, *Journal of  
775 Geophysical Research: Atmospheres*, 121, 2476-2489, 2016.
- 776 Wang, X., Wang, H., Xue, L., Wang, T., Wang, L., Gu, R., Wang, W., Tham, Y. J., Wang,



- 777 Z., Yang, L., Chen, J., and Wang, W.: Observations of  $\text{N}_2\text{O}_5$  and  $\text{ClNO}_2$  at a polluted  
778 urban surface site in North China: High  $\text{N}_2\text{O}_5$  uptake coefficients and low  $\text{ClNO}_2$   
779 product yields, *Atmospheric Environment*, 156, 125-134,  
780 10.1016/j.atmosenv.2017.02.035, 2017b.
- 781 Wang, X., Jacob, D. J., Eastham, S. D., Sulprizio, M. P., Zhu, L., Chen, Q., Alexander,  
782 B., Sherwen, T., Evans, M. J., Lee, B. H., Haskins, J. D., Lopez-Hilfiker, F. D., Thornton,  
783 J. A., Huey, G. L., and Liao, H.: The role of chlorine in global tropospheric chemistry,  
784 *Atmospheric Chemistry and Physics*, 19, 3981-4003, 10.5194/acp-19-3981-2019,  
785 2019b.
- 786 Wang, Z., Wang, W., Tham, Y. J., Li, Q., Wang, H., Wen, L., Wang, X., and Wang, T.:  
787 Fast heterogeneous  $\text{N}_2\text{O}_5$  uptake and  $\text{ClNO}_2$  production in power plant and industrial  
788 plumes observed in the nocturnal residual layer over the North China Plain,  
789 *Atmospheric Chemistry and Physics*, 17, 12361-12378, 2017c.
- 790 Wen, L., Xue, L., Wang, X., Xu, C., Chen, T., Yang, L., Wang, T., Zhang, Q., and Wang,  
791 W.: Summertime fine particulate nitrate pollution in the North China Plain: increasing  
792 trends, formation mechanisms and implications for control policy, *Atmospheric*  
793 *Chemistry and Physics*, 18, 11261-11275, 2018.
- 794 Wild, R. J., Edwards, P. M., Bates, T. S., Cohen, R. C., de Gouw, J. A., Dubé, W. P.,  
795 Gilman, J. B., Holloway, J., Kercher, J., Koss, A. R., Lee, L., Lerner, B. M., McLaren,  
796 R., Quinn, P. K., Roberts, J. M., Stutz, J., Thornton, J. A., Veres, P. R., Warneke, C.,  
797 Williams, E., Young, C. J., Yuan, B., Zarzana, K. J., and Brown, S. S.: Reactive nitrogen  
798 partitioning and its relationship to winter ozone events in Utah, *Atmos. Chem. Phys.*,  
799 16, 573-583, <https://doi.org/10.5194/acp-16-573-2016>, 2016.
- 800 Xia, M., Wang, W., Wang, Z., Gao, J., Li, H., Liang, Y., Yu, C., Zhang, Y., Wang, P.,  
801 Zhang, Y., Bi, F., Cheng, X., and Wang, T.: Heterogeneous Uptake of  $\text{N}_2\text{O}_5$  in Sand  
802 Dust and Urban Aerosols Observed during the Dry Season in Beijing, *Atmosphere*, 10,  
803 204, 2019.
- 804 Xia, M., Peng, X., Wang, W., Yu, C., Sun, P., Li, Y., Liu, Y., Xu, Z., Wang, Z., Xu, Z.,  
805 Nie, W., Ding, A., and Wang, T.: Significant production of  $\text{ClNO}_2$  and possible source  
806 of  $\text{Cl}_2$  from  $\text{N}_2\text{O}_5$  uptake at a suburban site in eastern China, *Atmospheric Chemistry*  
807 *and Physics*, 20, 6147-6158, 10.5194/acp-20-6147-2020, 2020.
- 808 Xue, L., Saunders, S., Wang, T., Gao, R., Wang, X., Zhang, Q., and Wang, W.:  
809 Development of a chlorine chemistry module for the Master Chemical Mechanism,  
810 *Geoscientific Model Development*, 8, 3151-3162, 2015.
- 811 Yan, C., Tham, Y. J., Zha, Q., Wang, X., Xue, L., Dai, J., Wang, Z., and Wang, T.: Fast  
812 heterogeneous loss of  $\text{N}_2\text{O}_5$  leads to significant nighttime  $\text{NO}_x$  removal and nitrate  
813 aerosol formation at a coastal background environment of southern China, *Science of*  
814 *The Total Environment*, 677, 637-647, 2019.
- 815 Yun, H., Wang, T., Wang, W., Tham, Y. J., Li, Q., Wang, Z., and Poon, S.: Nighttime  
816  $\text{NO}_x$  loss and  $\text{ClNO}_2$  formation in the residual layer of a polluted region: Insights from  
817 field measurements and an iterative box model, *Science of the Total Environment*, 622,  
818 727-734, 2017.
- 819 Yun, H., Wang, W., Wang, T., Xia, M., Yu, C., Wang, Z., Poon, S. C. N., Yue, D., and  
820 Zhou, Y.: Nitrate formation from heterogeneous uptake of dinitrogen pentoxide during



821 a severe winter haze in southern China, *Atmospheric Chemistry and Physics*, 18,  
822 17515-17527, 10.5194/acp-18-17515-2018, 2018.

823 Zhang, F., Shang, X., Chen, H., Xie, G., Fu, Y., Wu, D., Sun, W., Liu, P., Zhang, C., Mu,  
824 Y., Zeng, L., Wan, M., Wang, Y., Xiao, H., Wang, G., and Chen, J.: Significant impact  
825 of coal combustion on VOCs emissions in winter in a North China rural site, *Science*  
826 of The Total Environment, 720, 137617,  
827 <https://doi.org/10.1016/j.scitotenv.2020.137617>, 2020.

828 Zhang, H., Li, H., Zhang, Q., Zhang, Y., Zhang, W., Wang, X., Bi, F., Chai, F., Gao, J.,  
829 and Meng, L.: Atmospheric Volatile Organic Compounds in a Typical Urban Area of  
830 Beijing: Pollution Characterization, Health Risk Assessment and Source  
831 Apportionment, *Atmosphere*, 8, 61, 2017.

832 Zhou, W., Zhao, J., Ouyang, B., Mehra, A., Xu, W., Wang, Y., Bannan, T. J., Worrall, S.  
833 D., Priestley, M., and Bacak, A.: Production of N<sub>2</sub>O<sub>5</sub> and ClNO<sub>2</sub> in summer in urban  
834 Beijing, China, *Atmospheric Chemistry and Physics*, 18, 11581-11597, 2018.

835 Zhou, Y., Wang, T., Gao, X., Xue, L., Wang, X., Wang, Z., Gao, J., Zhang, Q., and Wang,  
836 W.: Continuous observations of water-soluble ions in PM<sub>2.5</sub> at Mount Tai (1534 m a.s.l.)  
837 in central-eastern China, *Journal of Atmospheric Chemistry*, 64, 107-127, 2009.